EDGE ARTICLE

Check for updates

Reversible dioxygen uptake at [Cu4] clusters†

Manasseh Kusi Osei,[a] Saber Mirzaei, [ID] [ab] M. Saeed Mirzaei,[a] Agustin Valles [ID] [a] and Raúl Hernández Sánchez [ID] *[ab]

Dioxygen binding solely through non-covalent interactions is rare. In living systems, dioxygen transport takes place *via* iron or copper-containing biological cofactors. Specifically, a reversible covalent interaction is established when O_2 binds to the mono or polynuclear metal center. However, O_2 stabilization in the absence of covalent bond formation is challenging and rarely observed. Here, we demonstrate a unique example of reversible non-covalent binding of dioxygen within the cavity of a well-defined synthetic all-Cu(I) tetracopper cluster.

Introduction

Reversible O_2 binding is the cornerstone of cellular respiration.[1] Hemoglobin, myoglobin, hemerythrin, and hemocyanin all serve as O_2 transporters across all living organisms.[2] In the process of biological uptake, transport, and delivery of dioxygen, a covalent bond is established between O_2 and Fe,[3] or similarly between O_2 and the Cu_2 site in hemocyanin,[4] resulting in charge transfer to form a superoxo or peroxo moiety, respectively. Although, non-covalent interactions have been described to be operative in stabilizing ferric–superoxo intermediates in heme proteins,[5] these nominally weak contacts are generally challenging to study.

Aside from biological cofactors, numerous studies have reported supramolecular complexes, porous materials, and organic cages capable of binding dioxygen. For instance, metal complexes formed within macrocyclic species, *e.g.*, palladium-bound cyclodextrin,[6] and Mn-supported calixarene,[7] lead to peroxo and superoxo moieties, respectively, stabilized inside the macrocycle. Similar occurrences are observed within metal organic frameworks (MOFs), where O_2 binding to embedded metal sites is used for O_2/N_2 separations,[8] or bond activation cleaving the O–O bond.[9,10] Last, macrocycles alone are also known to stabilize peroxo species.[11] However, to our knowledge, non-covalent interactions alone have not been described to stabilize neutral O_2 in biological metal cofactors or synthetic metal clusters. Here, we describe a polynuclear copper cluster built within a flexible supramolecular scaffold capable of

creating a unique pocket binding O_2 solely through non-covalent interactions.

Our group has developed modular amine-based ligands serving as templates for metal cluster formation. Recently, we reported a rigid ligand scaffold that enables the formation of square planar tetranuclear [Cu4] clusters (Fig. 1).[12] Keeping some of the design principles employed before, we decided to increase the degrees of freedom of the ligand scaffold as shown in Fig. 1. Others in the field have adopted similar measures either allowing or restricting the templating ligand's rigidity to alter the cluster reactivity and composition. For example, Betley and coworkers demonstrated that increasing the template's rigidity exchanging the tame ligand backbone (tame = 1,1,1-tris(aminomethyl)ethane),[13–16] for the tris-amine α-α-α-1,3,5-tris-aminocyclohexane,[17–19] opens the door for substrate activation pathways at trinuclear species not available in the former tame-based clusters. Similarly, C_3-symmetric 1,3,5-benzene substituted ligands developed by Holm to mimic iron sulfur

[a]Department of Chemistry, Rice University, 6100 Main St., Houston, Texas, USA. E-mail: raulhs@rice.edu

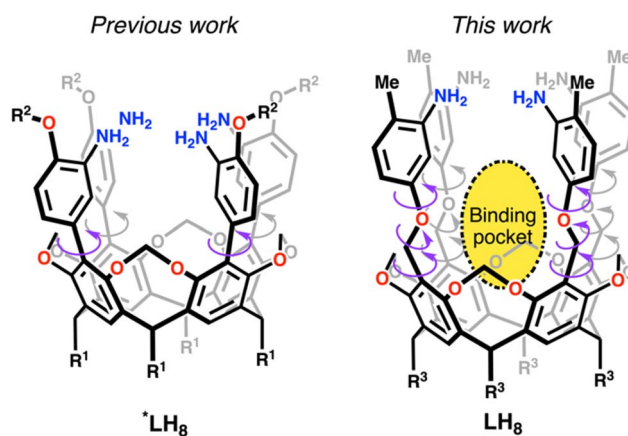*[b]Department of Chemistry, University of Pittsburgh, 219 Parkman Ave., Pittsburgh, Pennsylvania, 15260, USA*

Fig. 1 Previous ligand architecture *LH8 (R¹ = *n*-pentyl; R² = Me, Ph, or i-Bu) compared to LH8 (R³ = *n*-heptyl) reported herein with increased degrees of freedom.

clusters,[20,21] inspired the synthesis of oxygen-donor congeners in work reported by Agapie and coworkers towards the creation of Mn_3Ca subsite mimics of the oxygen evolving complex.[22–24] Most recently, Suess *et al.* using a similar ligand base fragment developed a nitrogen-donor analogue capable of isolating an iron sulfur alkyl cluster which mimics elusive enzymatic intermediates.[25,26] Other systems benefiting from ligand rigidification include those from the Murray group, whereupon limiting the degrees of freedom of their initial cryptand design,[27] they uncovered $[M_3]$ clusters, M = Fe, Co, Cu, and Zn, capable of ligating and activating N_2 and CO_2.[28–34] In our case, by increasing the degrees of freedom of our ligand scaffold we have created a binding pocket within an all-Cu(I) $[Cu_4]$ cluster that binds dioxygen through non-covalent interactions.

Results and discussion

Synthetic procedures

Our synthetic protocol provides square planar copper clusters in three steps from **1**, a precursor obtained readily in gram-scale quantities,[35] as shown in Scheme 1. First, a four-fold S_N2 reaction on **1** by 4-methyl-3-nitrophenol in basic conditions using K_2CO_3 in DMF for 24 hours produces ligand precursor $L(NO_2)_4$ in 64% isolated yield. This tetranitro species is reduced under 60 psi of H_2 over Pd/C in refluxing THF for 48 h. The reaction is quantitative by ^{1}H NMR; however, after work up the isolated yield of LH_8 is 97%. *In situ* deprotonation and metalation of this tetraamine ligand with $Cu_4(Mes)_4(py)_2$ in THF forms the all-Cu(I) diamagnetic species LH_4Cu_4 in 63% yield. ^{1}H NMR analysis of LH_4Cu_4 reveals its ideal C_{4v} symmetry in solution (Fig. S11†).

Cluster topology

Single crystal X-ray diffraction data was collected on crystals grown by vapor diffusion of pentane into a concentrated solution of LH_4Cu_4 in THF. The molecular structure of LH_4Cu_4 confirmed the formation of a square planar arrangement of Cu atoms sitting at an average distance d_{avg} (Cu–Cu) of 2.69(2) Å (Fig. 2a). For comparison, in Cu metal the Cu–Cu distance in Cu(100) is 2.55(1) Å.[36] Additionally, the $[Cu_4]$ core displays a d_{avg}

(Cu–N) of 1.89(1) Å and an almost linear local Cu coordination environment with an average $\angle$N–Cu–N of 177.3(7) degrees. Similar square-shaped tetranuclear copper clusters mimicking Cu_Z in N_2O reductase[37] have been previously reported by Mankad and coworkers using bridging diphosphine[38,39] or formamidinate[40–42] ligands resulting in cluster cores with Cu–Cu distances ranging from around 2.4 to 3.5 Å across all compounds reported therein. In fact, a recent example by the same group demonstrates the formation of a $[Cu_4(O_2)]$ adduct, where O_2 is bound to a single metal site.[43]

LH_4Cu_4 is closely related to our previously reported $[Cu_4]$ clusters;[12,44] however, we hypothesized that a larger internal cavity should be created in this newly synthesized cluster located in between the $[Cu_4N_4]$ fragment and the resorcinarene backbone as a consequence of the axially longer LH_8 relative to $*LH_8$. Our hypothesis was confirmed upon analyzing the molecular crystal structure obtained when LH_4Cu_4 is exposed to MeCN (Fig. 2b). The MeCN molecule is hosted below the $[Cu_4]$ plane establishing a $[Cu_4]$ centroid-to-N_{MeCN} distance of 3.852 Å. Note that the structure metrics of $LH_4Cu_4(MeCN)$ are relatively unchanged (d_{avg} (Cu–Cu) = 2.678(5) Å, d_{avg} (Cu–N) = 1.890(3) Å, $\angle$N–Cu–N = 177.4(6) degrees) from LH_4Cu_4.

Host–guest properties

Titration of MeCN to LH_4Cu_4 provided insight into the hydrogen atom resonances involved in the non-covalent bonding of MeCN in the host–guest adduct $LH_4Cu_4(MeCN)$. As observed in Fig. 3a, the addition of MeCN in $CDCl_3$ leads to resonance shifts in the ^{1}H NMR. Particularly noteworthy is that protons a, b, and c, as labeled in Scheme 1, shift downfield as equivalents of MeCN are added (Fig. S15† contains the full spectrum), a well-known effect for H atoms involved in hydrogen bonding.[45,46] The ^{1}H NMR spectrum additionally reveals the location of the MeCN signal at −1.76 ppm. Similar upfield shifts or shielding of the methyl resonance in acetonitrile has been observed in calixarene-based copper clusters.[47] Moreover, the stepwise addition of MeCN to LH_4Cu_4 produces a new set of resonances corresponding to $LH_4Cu_4(MeCN)$ while the location of those for LH_4Cu_4 remain unchanged, indicating a large host–guest association constant ($K_a > 10^5$ M^{-1} in $CDCl_3$)
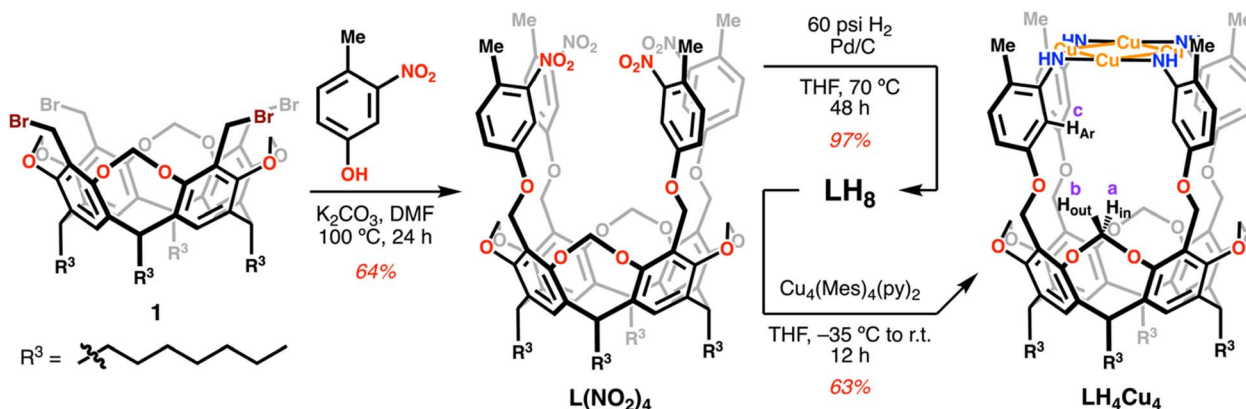
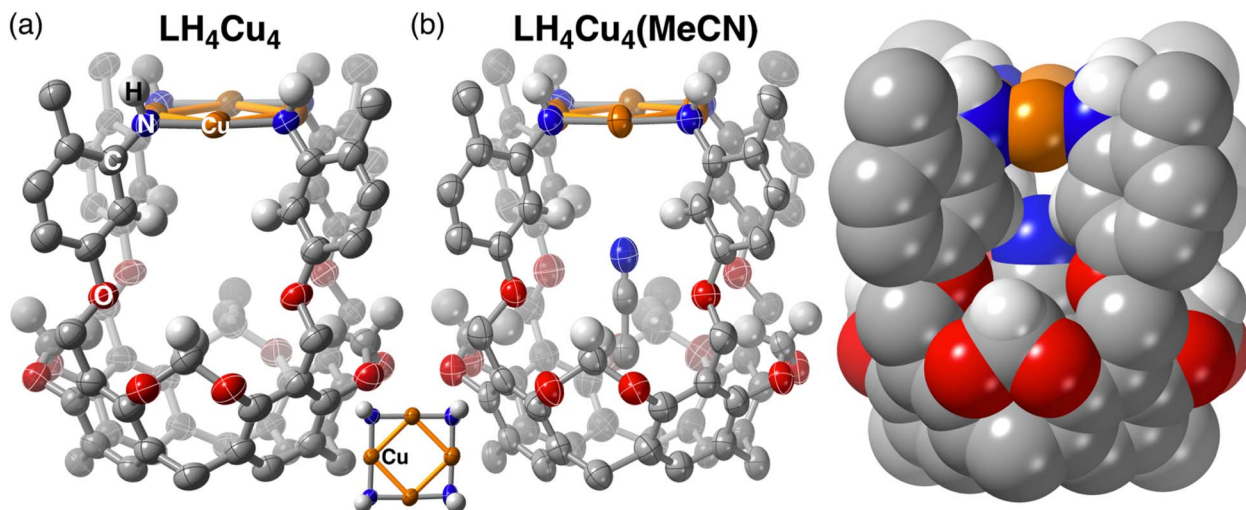**Scheme 1** Synthetic pathway for ligand LH_8 and metalation conditions leading to LH_4Cu_4.

Fig. 2 Molecular crystal structure of (a) **LH$_4$Cu$_4$** (100 K) and (b) **LH$_4$Cu$_4$(MeCN)** (100 K). Sphere packing model is shown for **LH$_4$Cu$_4$(MeCN)** to showcase the congested nature of its internal cavity. The C, N, O, Cu, and H atoms are coloured grey, blue, red, orange, and white, respectively. R groups (*n*-heptyl) and most hydrogen atoms, except for select ones, are omitted for clarity. Thermal ellipsoids are set at 50% probability level.

that goes beyond the measurable range *via* NMR.[48] Variable-temperature ^{1}H NMR in C$_6$D$_6$ provided insight into the thermodynamics of MeCN dissociation from **LH$_4$Cu$_4$(MeCN)** (Fig. S16†). A van't Hoff analysis reveals a dissociation enthalpy and entropy of 12.7 kcal mol^{-1} and 25.4 cal mol^{-1} K^{-1} (Fig. S17†), respectively. The calculated binding free energy of -5.14 kcal mol^{-1} at 298 K is similar to solvent binding in cavitands.[49] Most importantly, structural fidelity of **LH$_4$Cu$_4$(MeCN)** in combination with the ^{1}H NMR spectroscopic signatures resulting from MeCN binding provides a roadmap to investigate binding of other guests to **LH$_4$Cu$_4$**.

Copper–dioxygen chemistry is cornerstone in living systems and has inspired the realization of many synthetic compounds seeking to replicate its structure and function.[50,51] Seeking to probe potential ligation and activation modes of O$_2$ at **LH$_4$Cu$_4$**, an all-Cu(I) cluster, we dosed dry O$_2$ to an air-free solution of

LH$_4$Cu$_4$ in CDCl$_3$. As the atmosphere is exchanged from N$_2$ (Fig. 3b bottom) to O$_2$ (Fig. 3b middle), we observe broadening in proton resonances a, b, c, and the methine at 4.85 ppm. Note that the same proton resonances a, b, and c, are affected during MeCN binding. These proton resonances sharpen back when the O$_2$ atmosphere is removed (Fig. 3b top). Altogether, our experiments indicate that O$_2$ is reversibly accommodated in the same binding pocket as MeCN. Note that **L(NO$_2$)$_4$** and **LH$_8$** do not show any broadening of resonances a, b, and c under the same conditions (Fig. S19 and S20†). It is important to highlight that the vast majority of synthetic molecular [Cu^I_n] systems, with nuclearities ranging from $n = 1$ to 4, engage O$_2$ by establishing a copper–oxygen covalent bond giving rise to terminal or bridging peroxo, superoxo, or oxo complexes.[52] To the best of our knowledge, this is the first formally all-Cu(I) cluster reversibly binding O$_2$ solely *via* non-covalent interactions.
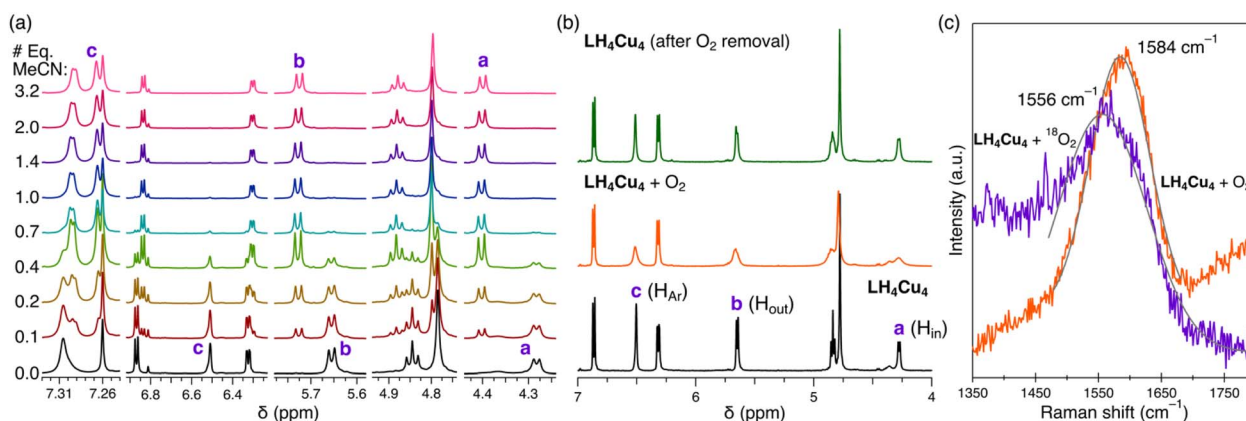

Fig. 3 (a) ^{1}H NMR spectra indicating resonances a, b, and c as MeCN is titrated into **LH$_4$Cu$_4$** in CDCl$_3$ at room temperature under a dinitrogen atmosphere. (b) Sequence of ^{1}H NMR spectra of **LH$_4$Cu$_4$** collected under N$_2$ (bottom), 1 atm of O$_2$ (middle), and last reverting back to N$_2$ (top). (c) Variable isotope resonance Raman spectra of **LH$_4$Cu$_4$** plus O$_2$ collected at room temperature. The region expected for the O−O stretch is shown. Partial fits (in grey) of the orange and purple traces to Gaussian curves served to locate the maximum.
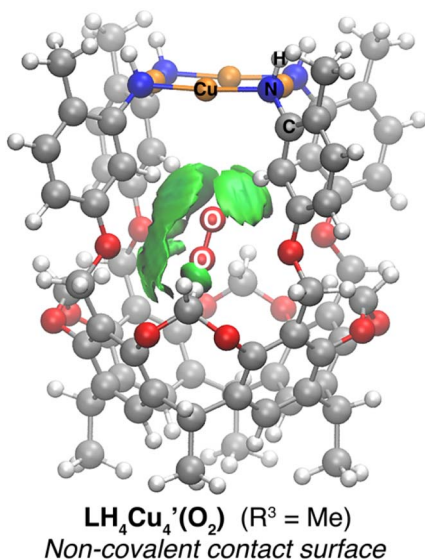
LH$_4$Cu$_4$'(O$_2$) (R^3 = Me)
Non-covalent contact surface

Fig. 4 IGMH map displaying the non-covalent interactions between O$_2$ and **LH$_4$Cu$_4$** (isovalue = 0.0011 a.u.).

Further examination of O$_2$ binding to **LH$_4$Cu$_4$** was carried out by collecting resonance Raman vibrational spectra on dried thin films of **LH$_4$Cu$_4$** contained within a quartz cuvette either under vacuum or dry dioxygen atmosphere. Laser excitation at 532 nm gave a band centered at 1584 cm^{-1} assigned to the O–O stretching of dioxygen hosted within **LH$_4$Cu$_4$** (Fig. 3c). Note that the symmetrical stretching band in free O$_2$ appears at 1556.4 cm^{-1} (Fig. S22†).[53] The same set of experiments were executed using isotopically labeled ^{18}O$_2$ displaying a stretching band at 1556 cm^{-1}. The simple harmonic oscillator model predicts a shift of ~90 cm^{-1}, however we only observe a Δ^{18}O of 28 cm^{-1}.[52] We hypothesize that dioxygen enters the cavity of **LH$_4$Cu$_4$** likely through partial ligand dissociation or *via* the formation of a dilated aperture.[54,55] Altogether, it appears that the non-covalent interactions serve to stabilize the O$_2$ molecule within **LH$_4$Cu$_4$** and at the same time strengthens the O–O bond by removing π^* electron density.

To further investigate the electronic properties of **LH$_4$Cu$_4$** and its adduct with O$_2$, we employed density functional theory (DFT) methods. **LH$_4$Cu$'_4$**(R^3 = Me) was optimized at B3LYP-D3BJ/Def2-SVP+PCM(CHCl$_3$) level of theory. The optimized structure reproduced the experimental data with high accuracy as determined by overlaying these structures and obtaining a root mean square displacement (RMSD) of 0.3 Å and d_{avg} (Cu–Cu) of 2.67 Å (Fig. S23†), indicating the reliability of the selected method.

Intrigued by the non-covalent binding of O$_2$ to **LH$_4$Cu$_4$**, the adduct **LH$_4$Cu$'_4$(O$_2$)** was first optimized employing B3LYP-D3BJ/Def2-SVP+PCM(CHCl$_3$) level of theory. The binding pocket within **LH$_4$Cu$'_4$** is best visualized by applying the independent gradient model based on Hirshfeld partition of molecular density (IGMH),[56] which clearly reveals the contact surface of weak non-covalent interactions involved in hosting the O$_2$ molecule. Note that the oxygen molecule positions itself in a way to maximize interactions with the C–H bonds from the bridging methylenes and top aromatic rings, protons a and c, respectively, in Scheme 1. The O$_2$

molecule was placed at different starting positions during structure optimization, *e.g.*, close to the resorcin[4]arene base, near the Cu$_4$ plane, and in all cases the optimum location found is that shown in Fig. 4. Overall, the IGMH isosurface for the O$_2$ adduct is well supported experimentally as reflected in the ^{1}H NMR data shown in Fig. 3b.

Conclusions

Here, we designed a novel ligand architecture carrying four aniline moieties to obtain a rigidified square-planar [Cu$_4$] topology despite the ligand's rotational degrees of freedom. The foregoing results show that, changing the resorcinarene backbone employed previously by our group engenders a cluster compound with a cavity to encapsulate small molecules, where we showcase a unique example of reversible non-covalent binding of O$_2$ within the [Cu$_4$] cluster built around a supramolecular scaffold.

Data availability

All data including experimental and analytical details are in the ESI.†

Author contributions

Manasseh K. Osei: conceptualization, investigation, data curation, writing – review & edition. Saber Mirzaei: conceptualization, investigation, data curation, formal analysis, writing – review & edition. M. Saeed Mirzaei: investigation, data curation, formal analysis. Agustin Valles: investigation. Raúl Hernández Sánchez: conceptualization, project administration, resources, funding acquisition, supervision, visualization, writing – original draft, writing – review & edition.

Conflicts of interest

There are no conflicts to declare.

Acknowledgements

Notes and references

1 G. T. Babcock, *Proc. Natl. Acad. Sci. U. S. A.*, 1999, **96**, 12971–12973.

2 J. S. Olson, *Antioxid. Redox Signaling*, 2019, **32**, 228–246.

3 A. Decker and E. I. Solomon, *Curr. Opin. Chem. Biol.*, 2005, **9**, 152–163.

4 D. A. Quist, D. E. Diaz, J. J. Liu and K. D. Karlin, *JBIC, J. Biol. Inorg. Chem.*, 2017, **22**, 253–288.

5 X. Huang and J. T. Groves, *Chem. Rev.*, 2018, **118**, 2491–2553.

6 R. Gramage-Doria, D. Armspach, D. Matt and L. Toupet, *Chem.–Eur. J.*, 2012, **18**, 10813–10816.

7 L.-L. Liu, H.-X. Li, L.-M. Wan, Z.-G. Ren, H.-F. Wang and J.-P. Lang, *Chem. Commun.*, 2011, **47**, 11146–11148.

8 E. D. Bloch, L. J. Murray, W. L. Queen, S. Chavan, S. N. Maximoff, J. P. Bigi, R. Krishna, V. K. Peterson, F. Grandjean, G. J. Long, B. Smit, S. Bordiga, C. M. Brown and J. R. Long, *J. Am. Chem. Soc.*, 2011, **133**, 14814–14822.

9 K. Hou, J. Börgel, H. Z. H. Jiang, D. J. SantaLucia, H. Kwon, H. Zhuang, K. Chakarawet, R. C. Rohde, J. W. Taylor, C. Dun, M. V. Paley, A. B. Turkiewicz, J. G. Park, H. Mao, Z. Zhu, E. E. Alp, J. Zhao, M. Y. Hu, B. Lavina, S. Peredkov, X. Lv, J. Oktawiec, K. R. Meihaus, D. A. Pantazis, M. Vandone, V. Colombo, E. Bill, J. J. Urban, R. D. Britt, F. Grandjean, G. J. Long, S. DeBeer, F. Neese, J. A. Reimer and J. R. Long, *Science*, 2023, **382**, 547–553.

10 X. He, A. Iliescu, T. Yang, M. Q. Arguilla, T. Chen, H. J. Kulik and M. Dincă, *J. Am. Chem. Soc.*, 2023, **145**, 16872–16878.

11 N. Lopez, D. J. Graham, R. McGuire, G. E. Alliger, Y. Shao-Horn, C. C. Cummins and D. G. Nocera, *Science*, 2012, **335**, 450.

12 M. K. Osei, S. Mirzaei, X. Bogetti, E. Castro, M. A. Rahman, S. Saxena and R. Hernández Sánchez, *Angew. Chem., Int. Ed.*, 2022, **61**, e202209529.

13 Q. L. Zhao and T. A. Betley, *Angew. Chem., Int. Ed.*, 2011, **50**, 709–712.

14 A. R. Fout, Q. L. Zhao, D. N. J. Xiao and T. A. Betley, *J. Am. Chem. Soc.*, 2011, **133**, 16750–16753.

15 T. D. Harris and T. A. Betley, *J. Am. Chem. Soc.*, 2011, **133**, 13852–13855.

16 E. V. Eames and T. A. Betley, *Inorg. Chem.*, 2012, **51**, 10274–10278.

17 T. M. Powers, A. R. Fout, S. L. Zheng and T. A. Betley, *J. Am. Chem. Soc.*, 2011, **133**, 3336–3338.

18 A. K. Bartholomew, C. E. Juda, J. N. Nessralla, B. Lin, S. G. Wang, Y.-S. Chen and T. A. Betley, *Angew. Chem., Int. Ed.*, 2019, **58**, 5687–5691.

19 T. M. Powers and T. A. Betley, *J. Am. Chem. Soc.*, 2013, **135**, 12289–12296.

20 T. D. P. Stack and R. H. Holm, *J. Am. Chem. Soc.*, 1987, **109**, 2546–2547.

21 T. D. P. Stack, J. A. Weigel and R. H. Holm, *Inorg. Chem.*, 1990, **29**, 3745–3760.

22 E. Y. Tsui, M. W. Day and T. Agapie, *Angew. Chem., Int. Ed.*, 2011, **50**, 1668–1672.

23 E. Y. Tsui, J. S. Kanady, M. W. Day and T. Agapie, *Chem. Commun.*, 2011, **47**, 4189–4191.

24 J. S. Kanady, E. Y. Tsui, M. W. Day and T. Agapie, *Science*, 2011, **333**, 733–736.

25 A. McSkimming and D. L. L. Suess, *Inorg. Chem.*, 2018, **57**, 14904–14912.

26 M. Ye, N. B. Thompson, A. C. Brown and D. L. Suess, *J. Am. Chem. Soc.*, 2019, **141**, 13330–13335.

27 G. L. Guillet, F. T. Sloane, M. F. Dumont, K. A. Abboud and L. J. Murray, *Dalton Trans.*, 2012, **41**, 7866–7869.

28 L. J. Murray, W. W. Weare, J. Shearer, A. D. Mitchell and K. A. Abboud, *J. Am. Chem. Soc.*, 2014, **136**, 13502–13505.

29 Y. Lee, F. T. Sloane, G. Blondin, K. A. Abboud, R. Garcia-Serres and L. J. Murray, *Angew. Chem., Int. Ed.*, 2015, **54**, 1499–1503.

30 D. M. Ermert, I. Ghiviriga, V. J. Catalano, J. Shearer and L. J. Murray, *Angew. Chem., Int. Ed.*, 2015, **54**, 7047–7050.

31 Y. Lee, K. J. Anderton, F. T. Sloane, D. M. Ermert, K. A. Abboud, R. García-Serres and L. J. Murray, *J. Am. Chem. Soc.*, 2015, **137**, 10610–10617.

32 B. J. Cook, G. N. Di Francesco, K. A. Abboud and L. J. Murray, *J. Am. Chem. Soc.*, 2018, **140**, 5696–5700.

33 R. B. Ferreira, B. J. Cook, B. J. Knight, V. J. Catalano, R. García-Serres and L. J. Murray, *ACS Catal.*, 2018, **8**, 7208–7212.

34 M. C. Eaton, V. J. Catalano, J. Shearer and L. J. Murray, *J. Am. Chem. Soc.*, 2021, **143**, 5649–5653.

35 R. Wu, T. F. Al-Azemi and K. S. Bisht, *RSC Adv.*, 2014, **4**, 16864–16870.

36 I.-K. Suh, H. Ohta and Y. Waseda, *J. Mater. Sci.*, 1988, **23**, 757–760.

37 T. Rasmussen, B. C. Berks, J. Sanders-Loehr, D. M. Dooley, W. G. Zumft and A. J. Thomson, *Biochemistry*, 2000, **39**, 12753–12756.

38 B. J. Johnson, S. V. Lindeman and N. P. Mankad, *Inorg. Chem.*, 2014, **53**, 10611–10619.

39 C.-W. Hsu, S. C. Rathnayaka, S. M. Islam, S. N. MacMillan and N. P. Mankad, *Angew. Chem., Int. Ed.*, 2020, **59**, 627–631.

40 B. J. Johnson, W. E. Antholine, S. V. Lindeman and N. P. Mankad, *Chem. Commun.*, 2015, **51**, 11860–11863.

41 B. J. Johnson, W. E. Antholine, S. V. Lindeman, M. J. Graham and N. P. Mankad, *J. Am. Chem. Soc.*, 2016, **138**, 13107–13110.

42 S. C. Rathnayaka, C. W. Hsu, B. J. Johnson, S. J. Iniguez and N. P. Mankad, *Inorg. Chem.*, 2020, **59**, 6496–6507.

43 N. P. Mankad, *Chem. Sci.*, 2024, **15**, 1820–1828.

44 **LH$_4$Cu$_4$** also displays an irreversible oxidation near 0 V *vs.* Fc/Fc$^+$ (Fig. S13†).

45 K. Choi and A. D. Hamilton, *J. Am. Chem. Soc.*, 2003, **125**, 10241–10249.

46 S. Mirzaei, V. M. Espinoza Castro and R. Hernández Sánchez, *Chem. Sci.*, 2022, **13**, 2026–2032.

47 N. Frank, A. Dallmann, B. Braun-Cula, C. Herwig and C. Limberg, *Angew. Chem., Int. Ed.*, 2020, **59**, 6735–6739.

48 P. Thordarson, *Chem. Soc. Rev.*, 2011, **40**, 1305–1323.

49 O. Dumele, N. Trapp and F. Diederich, *Angew. Chem., Int. Ed.*, 2015, **54**, 12339–12344.

50 C. Wurtele, E. Gaoutchenova, K. Harms, M. C. Holthausen, J. Sundermeyer and S. Schindler, *Angew. Chem., Int. Ed.*, 2006, **45**, 3867–3869.

51 E. I. Solomon, D. E. Heppner, E. M. Johnston, J. W. Ginsbach, J. Cirera, M. Qayyum, M. T. Kieber-

Emmons, C. H. Kjaergaard, R. G. Hadt and L. Tian, *Chem. Rev.*, 2014, **114**, 3659–3853.

52 C. E. Elwell, N. L. Gagnon, B. D. Neisen, D. Dhar, A. D. Spaeth, G. M. Yee and W. B. Tolman, *Chem. Rev.*, 2017, **117**, 2059–2107.

53 H. G. M. Edwards, D. A. Long, K. A. B. Najm and M. Thomsen, *J. Raman Spectrosc.*, 1981, **10**, 60–63.

54 A. V. Davis and K. N. Raymond, *J. Am. Chem. Soc.*, 2005, **127**, 7912–7919.

55 S. Rieth, Z. Yan, S. Xia, M. Gardlik, A. Chow, G. Fraenkel, C. M. Hadad and J. D. Badjić, *J. Org. Chem.*, 2008, **73**, 5100–5109.

56 T. Lu and Q. Chen, *J. Comput. Chem.*, 2022, **43**, 539–555.